Chem

CellPress

Article

Precise synthesis of non-equilibrium rotaxanes via pumping in water

Guangcheng Wu,[1,2,13,*] Jihye Park,[3,4] Wei-Guang Liu,[5] Yang Jiao,[2] Long Zhang,[2] Han Han,[1,2] Chun Tang,[1,2] Taehwan Jang,[3] Minho M. Kim,[3] Bo Song,[2] Xuesong Li,[2,6] Ruihua Zhang,[1,2] Enxu Liu,[1] Huang Wu,[1,2] Yong Wu,[1,2] Xingang Zhao,[2] Yuanning Feng,[2] Qing Li,[7] Hyungjun Kim,[3] R. Dean Astumian,[8,*] William A. Goddard III,[5,*] and J. Fraser Stoddart[1,2,9,10,11,12,*]

[1]Department of Chemistry, The University of Hong Kong, Hong Kong SAR 999077, China
[2]Department of Chemistry, Northwestern University, Evanston, IL 60208, USA
[3]Department of Chemistry, Korea Advanced Institute of Science and Technology, Daejeon 34141, Republic of Korea
[4]Materials Science Division, Lawrence Berkeley National Laboratory, Berkeley, CA 94720, USA
[5]Materials and Process Simulation Center, California Institute of Technology, Pasadena, CA 91125, USA
[6]Department of Chemistry, University of Wyoming, Laramie, WY 82072, USA
[7]Key Laboratory of Macrocyclic and Supramolecular Chemistry of Guizhou Province, Institute of Applied Chemistry, Guizhou University, Guiyang, Guizhou 550025, China
[8]Department of Physics and Astronomy, University of Maine, Orono, ME 04473, USA
[9]Center for Regenerative Nanomedicine, Northwestern University, Chicago, IL 60611, USA
[10]Stoddart Institute of Molecular Science, Department of Chemistry, Zhejiang University, Hangzhou, Zhejiang 310027, China
[11]ZJU-Hangzhou Global Scientific and Technological Innovation Center, Hangzhou, Zhejiang 311215, China
[12]School of Chemistry, University of New South Wales, Sydney, NSW 2052, Australia
[13]Lead contact
*Correspondence: gcwu2023@hku.hk (G.W.), astumian@maine.edu (R.D.A.), wag@caltech.edu (W.A.G.), stoddart@hku.hk (J.F.S.)
https://doi.org/10.1016/j.chempr.2025.102878

THE BIGGER PICTURE Life is sustained by microscopic machines that operate away from equilibrium, performing entropy-reducing tasks such as directional transport and the assembly of ordered structures. A long-standing goal of science has been to decipher the operating principles of these bio-machines, with the ultimate ambition of emulating—and even reprogramming—such functions on demand. In this pursuit, artificial molecular machines (AMMs) have emerged as a transformative, bottom-up alternative to their naturally evolved bio-counterparts, which often exhibit structural complexity and redundancy. Conceived from fundamental thermodynamic theories and rational chemical design, AMMs provide unparalleled functional diversity, enabling the creation of molecular devices with tailored properties not found in nature. However, examples of non-equilibrium operating AMMs remain rare to date, and even fewer can function in pure water, the solvent of life. This is because water is a strong solvent that stifles effectively the polar interactions that are employed rationally to orchestrate controlled motions at the molecular level. We herein report a brand-new design of artificial molecular pump (AMP) that operates effectively in pure water to drive the active transport of cucurbit[7]uril rings onto the polyethylene glycol chain of a molecular dumbbell. The number of rings incorporated is determined precisely by the number of pH oscillating cycles, enabling programmable synthesis of otherwise-inaccessible non-equilibrium mechanically interlocked polymers. This research not only enriches the toolbox of non-equilibrium molecular devices but also, in the long run, opens up avenues for integrating synthetic molecular machinery with biological systems, with potential implications from targeted therapeutic delivery to functional bio-hybrid materials and beyond.

SUMMARY

Water is the matrix of life in which biomolecular machines carry out vital functions through ordered mechanical movements. The controlled active transport in artificial systems within aqueous environments, however, remains challenging at the molecular level, resulting from the inherent difficulties in manipulating molecular motions accurately in water. Herein, we present artificial molecular pumps (AMPs) capable of forming and maintaining non-equilibrium concentration differences of cucurbit[7]uril rings (up to 350 times) in aqueous media. Acid-base neutralization energy is exploited to add efficiently and precisely one ring per cycle to

the dumbbells of both a solo and a duet pump by a rationally optimized pumping cassette. Operation is achieved under ambient conditions through simple pH modulation (2–7). A combination of kinetic investigations, computational modeling, and theoretical analysis provides a mechanistic understanding of how the aqueous AMPs harness chemical energy to produce and sustain high-energy oligorotaxanes in a non-equilibrium steady state.

INTRODUCTION

From a thermodynamic perspective, all life's processes hinge on states that lie away from equilibrium.[1] This requirement is met by the unremitting operations of biomolecular motors driving the system energetically uphill at the microscopic level. By consuming energy (usually provided by ATP or light), biomolecular motors enable directional motions and active transport and sustain concentration gradients of crucial substances across cellular compartments, contributing to ordered structures and vital functions.

Inspired by these natural systems, artificial molecular motors[2–18] and, more specifically, artificial molecular pumps[19–25] (AMPs) have emerged as minimalist-designed alternatives capable of the unidirectional motions and the active transport of desired molecular cargoes, including the unnatural ones. Their potential to operate within biological contexts has long motivated efforts to develop artificial molecular motors and pumps that function in aqueous media—"the matrix of life.[26,27]" This endeavor has yielded considerable progress, with pioneering demonstrations of function in environments ranging from membrane systems[28–36] or aqueous-organic solvents[6,37–42] to pure water.[43] Notable examples include carbodiimide-fueled motors,[6,35–41,43,44] which harness the hydration energy of carbodiimides to drive directional motions in aqueous environments, and light-driven rotary motors,[45–47] whose robust unidirectional rotation has been adapted for operation in pure water.

Notwithstanding these advances, the motional unidirectionality and operational accuracy of artificial systems still fall short of their biological counterparts,[48,49] limiting their utility in demanding applications such as targeted drug delivery[50] with mitigated systemic toxicity or precision assembly[51] of functional materials. Generally, such challenges are relatively hard to overcome in aqueous environments, where water's high polarity not only introduces dominant hydrophobic effects that complicate intercomponent dynamics but also attenuates significantly the electrostatic and other polar noncovalent interactions essential for sculpting the potential energy landscapes for Brownian ratchets.[52–55] A recent report[56] on a water-soluble variant of the well-established[57] redox-driven AMP described the efficient pumping of the cyclobis(paraquat-*p*-phenylene) rings in pure water, retaining the ability to produce poly[n]rotaxanes (n up to 3) in reasonable yield. This efficacy is attributed to its compositionally simple yet effective pumping cassette and energy ratchet mechanism,[58,59] which enables coherent assembling across all molecules in the ensemble. Nevertheless, the practical implementation of this system necessitates product separation between successive pumping cycles and meticulous control of anaerobic conditions, indicating significant room for improvement in operational accessibility and robustness.

Herein, we address these challenges by reporting the rational design, modular synthesis, and simple operation of AMPs capable of pumping cucurbit[7]uril (**CB7**) rings onto the dumbbell components of oligorotaxanes away from equilibrium in water. The highly efficient energy ratchet with minimal design enables the production of well-defined non-equilibrium oligorotaxanes, which are otherwise inaccessible owing to the lack of favorable interactions between the rings and the dumbbells. Remarkably, such quantitative assembling can be operated in a consecutive manner and is achieved simply by pulses of trifluoroacetic acid (protonation) and sodium hydroxide (deprotonation) without special needs for anaerobic conditions. Supported by fundamental theory, detailed kinetic studies and computational investigations have been performed in order to gain mechanistic insights into the stepwise pumping process in aqueous media.

RESULTS AND DISCUSSION

Design of an AMP operating in water

Cucurbiturils (**CB**s) are well known[60–65] for their ability to form extremely tight[66] complexes with positively charged organic guests in water, despite the presence of competitive solvation. This strong affinity benefits from the convergently arranged carbonyl groups at the portals of **CB**s showing cooperatively enhanced binding toward cations. Their highly negatively polarized portals engender substantial electrostatic repulsions against anionic species, leading to a starkly contrasting binding behavior of **CB**s in water based on the charge states of the guests (Figure 1A). This characteristic has enabled pH-responsive recognition[67,68] of **CB**s involving carboxylic-acid-containing guest molecules,[69–71] which we anticipated could serve as the basis for pH-driven energy ratchets, paving the way in the development of water-compatible AMPs. Additionally, **CB**s exhibit excellent biocompatibility[72] and versatile functionalization potential,[73,74] rendering them highly promising candidates as cargo for AMPs, particularly in the context of bio-oriented applications. **CB7** was chosen as the ring component in our investigation because of its outstanding recognition properties and reasonable water solubility.

Inspired by the minimalist design principles of the established redox-driven AMP[19,57] and based on a sequence of preliminary investigations (see supplemental information, Section S4), we have synthesized (Figure 1B) a water-compatible dumbbell-shaped molecular solo pump (**SP**). The molecular structure of **SP** features a polyethylene glycol (PEG) chain with a precise number of repeating units (24-mer) as the collecting chain that is terminated on one end by a pumping cassette and on the other end by a bulky pyranine stopper. The pumping cassette, whose charge state can be changed depending on pH, comprises a *p*-xylylene-diammonium recognition site linked to

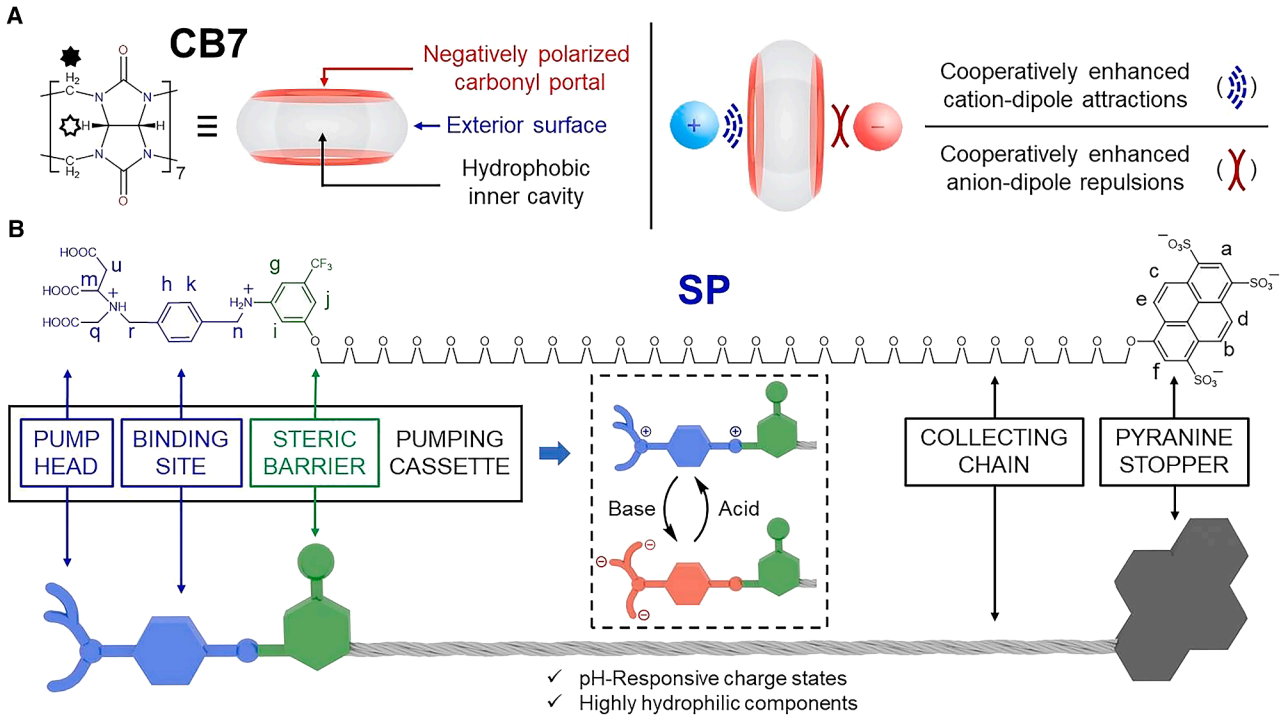

Figure 1. Design of an AMP operating in aqueous solution

(A) Graphical representations of a **CB7** ring showing its hydrophobic cavity, exterior surface, and negatively polarized portals, which display strongly contrasting interactions toward cations and anions. Methine protons on **CB7** are labeled with a black hollow star, while the methylene protons on **CB7** are labeled with a black solid star.

(B) Structural formulas and schematic representation of the molecular solo pump **SP**. Consisting of a tri-carboxylic acid pump head and a TFP steric barrier, connected to a diammonium binding site, the pumping cassette is linked to a PEG collecting chain comprising 24 repeating units and terminated by a pyranine stopper. The inset shows that the pumping cassette can switch between different charge states depending on the pH conditions. Counterions, including CF_3COO^- and Na^+, are omitted for the sake of clarity. Proton assignments relevant to the interpretation of the ^1H NMR spectra are provided.

a tri-carboxylic acid pump head at the interface with the bulk solution and a trifluoromethyl-substituted phenylene (TFP) ring acting as a steric barrier and connected covalently to the collecting chain. Because both the pumping cassette and the pyranine stopper are ionized under both acidic and basic conditions and the collecting chain is hydrophilic, **SP** is soluble (>20 mM) in water.

We hypothesized that under *acidic conditions*, driven by hydrophobic and cation-dipole interactions, the **CB7** ring will thread over the tri-carboxylic acid pump head to form a stable inclusion complex (Figure 2A) with the recognition site. Furthermore, under *basic conditions*, both the tri-carboxylic acid and *p*-xylylene-diammonium units will be deprotonated, and the co-conformation with **CB7** residing on the recognition site will no longer be stable because of the loss of stabilizing cation-dipole interactions and because of repulsion (Figure 2A) between the electron-rich carbonyl portal and the adjacent negatively charged tri-carboxylates pump head. This metastably trapped **CB7** ring will escape preferentially over the steric barrier to the collecting chain rather than over the pump head back into the bulk solution because the repulsion between the carbonyl portal on the **CB7** and the tri-carboxylates on the pump head is stronger than the hindrance resulting from the steric barrier. Consequently, the **CB7** ring becomes mechanically trapped on the collecting chain even though there are no stabilizing interactions, yielding (Figure 2A) a kinetically inert non-equilibrium [2]rotaxane. Effective progressive pumping requires that the kinetic barrier to the movement of **CB7** associated with the steric barrier must be higher than that associated with the protonated pump head while being lower than that of the deprotonated pump head. The TFP steric barrier fulfills these requirements (supplemental information, Section S4.2).

Pumping one CB7 ring at a time onto a solo pump SP

Loading the first **CB7** ring from bulk solution onto the pumping cassette was achieved by mixing **SP** (1.0 mM) and 1.5 equiv of **CB7** (1.5 mM) in D_2O acidified to pD = 2 with CF_3COOD. The relatively high 1:1 binding affinity ($7.31 \times 10^5\ M^{-1}$; see supplemental information, Section S5) between **CB7** and **SP** under acidic conditions guarantees the quantitative loading of a **CB7** ring onto the pumping cassette of **SP** without requiring a large excess of **CB7** present in the bulk solution. The ^1H NMR spectrum (Figure 2B) supports the exclusive complexation of **SP** with **CB7** immediately after mixing, showing the relatively fast threading kinetics of a **CB7** ring over the tri-carboxylic acid pump head onto the recognition site, although the free and bound species exchange (Figure S44) slowly on the ^1H NMR timescale. The resonances for H_g and H_j associated with the steric barrier on **SP**

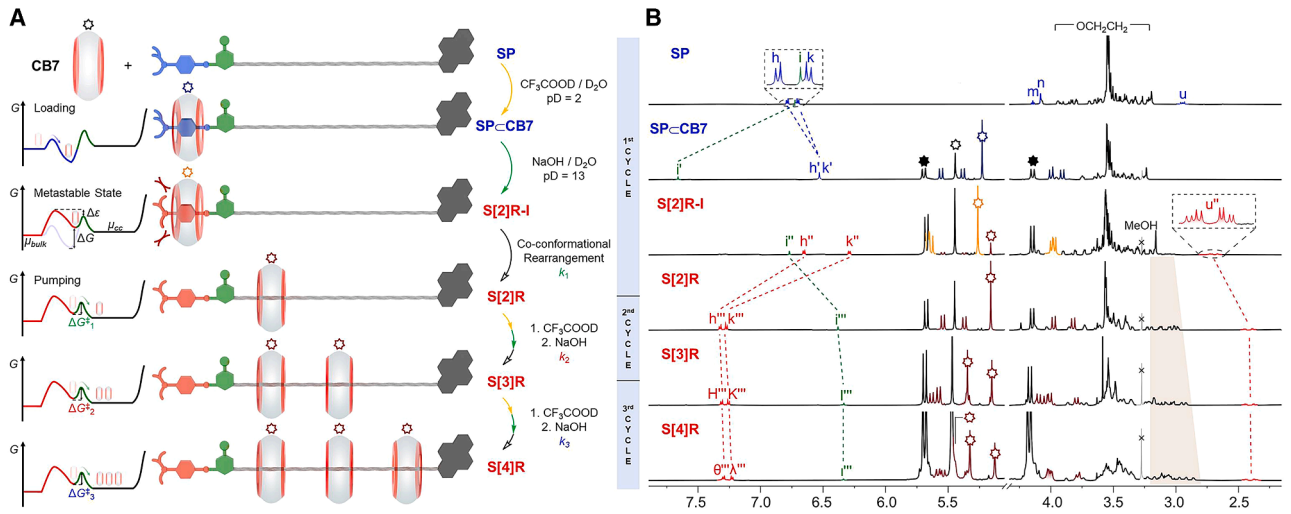

Figure 2. Graphical representations of the operating mechanism and the partial ^{1}H NMR spectroscopic characterization of the stepwise pumping of CB7 rings onto SP

(A) Graphical representation of the stepwise operation for the pH-driven pumping of **CB7** rings onto the solo pump **SP**, leading to the synthesis of a [4]rotaxane in water, with energy landscapes representing the free energies of the system at each selected stage. The curved arrows on the energy landscapes indicate the kinetically favored directions for the **CB7** ring moving along the dumbbell. Signals for **CB7**/CB7 in various chemical environments are differentiated by color: black (unbound), deep blue (**CB7**s encircling the protonated pumping cassette), orange (CB7s encircling the deprotonated pumping cassette), and deep red (CB7s residing on the collecting chain), respectively.

(B) Partial ^{1}H NMR spectra (600 MHz, D_2O, 298 K) of selected states over three pumping cycles. The spectra were obtained from three independent pumping experiments leading to the formation of **S[2]R**, **S[3]R**, and **S[4]R**, respectively. The key proton resonances have been assigned according to the labels in (A) and Figure 1. The high-field resonances for the PEG collecting chain protons are highlighted to show their upfield shift as more and more CB7s are accommodated on the **SP** dumbbell.

disappear in the ^{1}H NMR spectrum (Figure 2B) on account of deuteration under acidic conditions. The resonances for H_h and H_k on the recognition site shift upfield, while those for H_i on the steric barrier shift downfield—$\Delta\delta$ = 0.93 ppm—indicating that the *p*-phenylene recognition site is located inside the **CB7** cavity, while the TFP steric barrier remains outside, close to the carbonyl rim of **CB7**. The rotating-frame Overhauser effect spectroscopy (ROESY) spectrum (Figure S48) shows unambiguously the proximity of $H_{h'}$, $H_{k'}$, $H_{i'}$, and the protons on **CB7**. Further evidence of the complexation is observed (Figure S49) in the diffusion ordered spectroscopy (DOSY) spectrum, confirming the formation of a single species, namely **SP⊂CB7**.

Subsequent addition of NaOH in one batch, which basifies (pD $\geq$ 7) the solution, triggers the displacement of the **CB7** ring from the recognition site. Under basic conditions, the proton resonances (Figure 2B) in the aromatic region of the metastable species **S[2]R-I** occur in the same order as those of **SP⊂CB7** under acidic conditions. Note that in the **S[2]R-I** the resonance for proton $H_{h''}$ has moved downfield, consistent with the **CB7** ring having moved toward the TFP steric barrier, while $H_{k''}$ remains inside its cavity and $H_{h''}$ resides close to the carbonyl rim. The ^{1}H NMR spectrum (Figure S51) of the equilibrium state (>6 h), however, shows another set of CB7 resonances in addition to those for the free **CB7**, indicating that one CB7 ring is threaded onto the dumbbell. The upfield shift of the ^{1}H-resonances on the PEG collecting chain, together with the downfield shift of the resonances for the *p*-phenylene recognition site protons, all point to the fact that the **CB7** ring has passed over the TFP steric barrier and is trapped on the PEG collecting chain, forming a [2]rotaxane **S[2]R** as a result of this co-conformational change. This compound could be isolated by chromatography and was characterized by high-resolution mass spectrometry (HRMS) (Figure S59) and DOSY (Figure S57) as well as by a ROESY experiment (Figure S56) in which nOe correlations between the protons of the PEG collecting chain and CB7 could be observed. An nOe signal also exists between $H_{b''}$ on the pyranine stopper and the methine protons of the CB7 ring trapped on the collecting chain, suggesting a tendency for the stopper to associate with the exterior surface of the CB7 ring on account of the chaotropic effect.[75] Acronyms are displayed in bold when they represent a compound or a part of a complex. When they represent the component [ring or dumbbell] of a mechanically interlocked molecule, e.g., a rotaxane, they are presented in a plain text font.

^{19}F NMR spectroscopy (Figure S58) allows a simpler temporal monitoring of the pumping process. The intensity of the ^{19}F resonance in **S[2]R-I** decreases, while that for **S[2]R** increases gradually with time. No other species is observed in the equilibrium state by either ^{1}H or ^{19}F NMR spectroscopy. The integrations (Figure S54) of the resonances for CB7 and the dumbbell signals are in accord with 1:1 stoichiometry, suggesting the precision performance of pumping.

The fact that one **CB7** ring is installed on the PEG collecting chain of **SP** in one cycle of acidification (pD = 2) and basification (pD $\geq$ 7) encouraged us to explore the possibility of installing more rings to produce polyrotaxanes by means of subsequent pumping cycles. The installation of additional rings can be

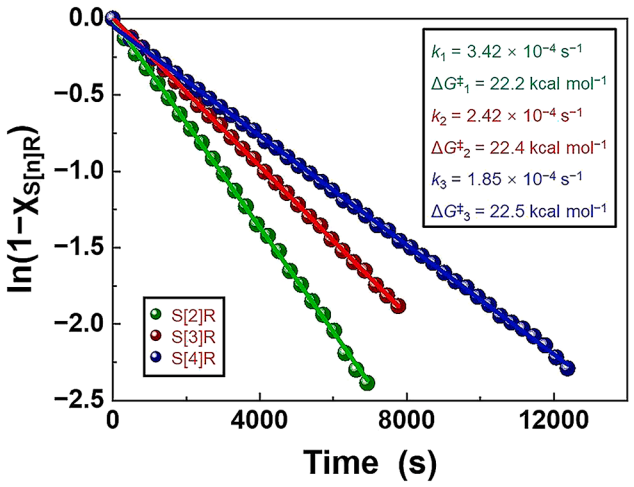

Figure 3. Kinetic plots for the co-conformational rearrangements for the three pumping cycles of SP

Plots obtained by tracking the molar ratios of **S[n]R** ($n = 2 \sim 4$) according to the integrals from the ^{1}H NMR spectra (600 MHz, D_2O, pD = 13, 298 K) monitored over time in three independent pumping experiments. The data are fitted according to first-order kinetics. The resulting k values are listed along with the derived $\Delta G^{\ddagger}$ values obtained from the Eyring equation.

accomplished in either a stepwise fashion with separation of products at each step or in a one-pot manner without isolation of intermediate products. Loading a **CB7** ring from the bulk solution onto the recognition site on **S[2]R** was achieved by acidifying its aqueous solution (pD = 2) with CF_3COOD in the presence of a slight excess of **CB7** in the bulk solution. The backward translocation of the CB7 ring from the PEG collecting chain is ignorable by virtue of the presence of the TFP steric barrier (supplemental information, Section S4.2). Pumping of the second ring onto the PEG collecting chain was realized by basifying ($pD \geq 7$) the solution with NaOH, giving rise (Figure S65) to the quantitative production of a [3]rotaxane **S[3]R**, which was identified by HRMS. Using the same protocol, a third **CB7** ring was pumped onto the PEG collecting chain, leading to the formation of the [4]rotaxane **S[4]R**. Fortunately, both **S[3]R** and **S[4]R** could be characterized in their ^{1}H NMR spectra (Figure 2B) by the number of singlets corresponding to the heterotopic methine protons on either the two or three CB7 rings residing on the PEG collecting chains. We attribute this observation to the limited length of the collecting chain, on which the trapped rings can associate with either end of the dumbbell through noncovalent interactions. Despite the CB7 rings retaining translational freedom, they experienced distinct chemical environments defined by the asymmetric terminals of the collecting chain. The resonances for the protons associated with the PEG collecting chain undergo further upfield shifts as more and more CB7 rings are trapped. 2D NMR spectroscopy confirmed that the structural assignments are consistent with them being [3]- and [4]rotaxanes. See supplemental information, Section S6 for more details.

Kinetic studies reveal that the first-order kinetic constants (Figure 3) for the first, second, and third **CB7** rings to pass over the TFP steric barrier are $k_1 = 3.42 \times 10^{-4}$ s^{-1}, $k_2 = 2.42 \times 10^{-4}$ s^{-1}, and $k_3 = 1.85 \times 10^{-4}$ s^{-1}, respectively, at 298 K under pD = 13, corresponding to activation barriers $\Delta G^{\ddagger}_1 = 22.2$ kcal mol^{-1}, $\Delta G^{\ddagger}_2 = 22.4$ kcal mol^{-1}, and $\Delta G^{\ddagger}_3 = 22.5$ kcal mol^{-1}, respectively. The fact that the activation energies are quite similar to one another indicates that the recruitment of **CB7** rings from the pumping cassette is not hindered by CB7 rings already installed on the PEG collecting chain, a situation that makes the progressive pumping of **CB7** rings away from equilibrium possible. All three rotaxanes are stable in basic aqueous solution for more than 6 months at room temperature, without loss of CB7 rings, confirming the effectiveness of the pyranine stopper and pumping cassette in trapping rings. We expect the pumping to continue with repeated cycles until the chemical potential difference between rings on the collecting chain and in the bulk attains the steady state value given by the non-equilibrium pumping equality[76]:

$$e^{(\mu_{cc} - \mu_{bulk})/RT} = \langle e^{\mathcal{W}_{pd}/RT} \rangle \qquad \text{(Equation 1)}$$

where $\mathcal{W}_{pd}$ is the path-dependent energy exchanged with the environment in a specific trajectory, and the angle brackets indicate an average over all paths for threading of a ring. In the context of Figure 2A the average for the two-state pumping is

$$\langle e^{\mathcal{W}_{pd}/RT} \rangle \approx \left[\frac{e^{\frac{(\Delta\varepsilon + \Delta G)}{RT}} + 1}{e^{\frac{\Delta\varepsilon}{RT}} + e^{\frac{\Delta G}{RT}}} \right] \qquad \text{(Equation 2)}$$

Pumping two CB7 rings simultaneously onto a duet pump DP

To investigate the total capacity of the PEG collecting chain to accommodate **CB7** rings, we synthesized a molecular duet pump (**DP**). The **DP** also contains a 24-mer PEG chain linking two pumping cassettes in a tail-to-tail manner. **DP** is capable of trapping precisely two **CB7** rings simultaneously on the collecting chain during each pumping cycle. The pumping of the first two rings is achieved using the protocol analogous to that for **SP**, which leads to the quantitative formation of the [3]rotaxane **D[3]R**. During this process, however, an intermediate (**D[3]R-II**) is formed, where one CB7 ring is already positioned on the collecting chain, while the other ring resides on the pumping cassette (Figure 4A), a situation that can be monitored over time by ^{1}H (and ^{19}F) NMR spectroscopy (Figures 4B and S92–S94). These results show that translocation of the two rings occurs asynchronously, where one ring from either cassette moves onto the collecting chain, followed by the other ring. Both steps follow first-order kinetics, and equations for the time dependence of the concentrations of **D[3]R-I** and **D[3]R-II** are presented (see supplemental information, Section S1.2.2) and used to fit the dynamic ^{1}H NMR spectroscopic data so as to obtain the kinetic/thermodynamic parameters associated with the two steps at 298 K under pD = 13 of $k_1 = 2.86 \times 10^{-4}$ s^{-1}, $\Delta G^{\ddagger}_1 = 22.3$ kcal mol^{-1}, and $k_2 = 2.50 \times 10^{-4}$ s^{-1}, $\Delta G^{\ddagger}_2 = 22.4$ kcal mol^{-1}, respectively. The activation barriers are very similar to those for the first and the second pumping cycles observed in the case of the solo pump. These results demonstrate that the thermodynamic properties of these AMPs are governed by the design of the pumping cassette. The second cycle of pumping—as anticipated—generates a [5]rotaxane, **D[5]R**,

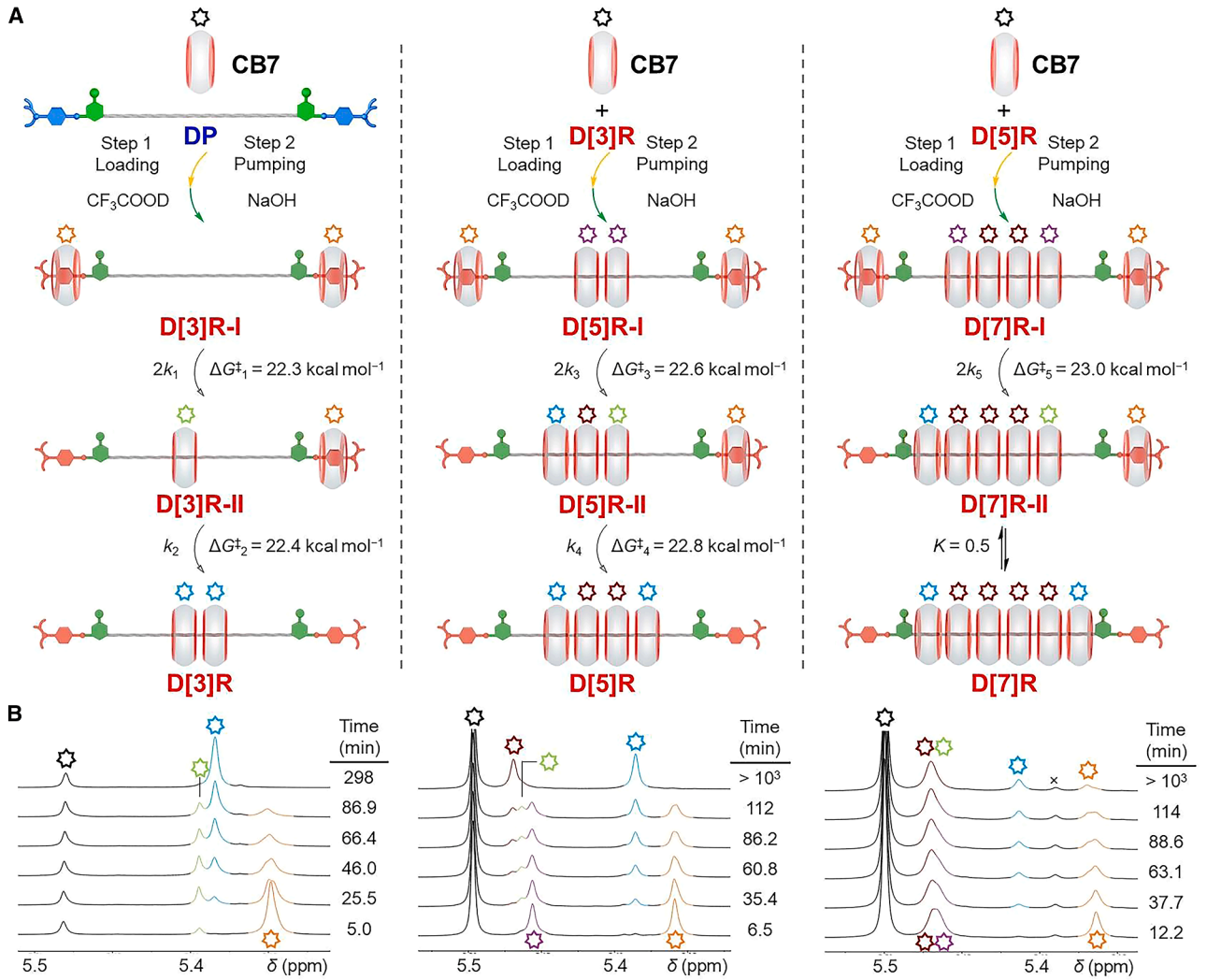

Figure 4. Graphical representations and kinetic analysis of the stepwise pumping of CB7 rings onto the DP dumbbell over three cycles

(A) Illustrations of the first (left), second (middle), and third (right) pumping cycles of the duet pump **DP**. In each cycle, two **CB7** rings are first of all loaded onto the two pumping cassettes at both ends in the presence of acid. Subsequent basification triggered the pumping of pairs of rings onto the PEG collecting chains in a two-step manner. Firstly, one of the two rings traverses over the TFP steric barrier since the initial metastable states **D[n]R-I** (n = 3, 5, 7) are symmetrical. Because the second steps are stereochemically different from those of the first ones, the two kinetic parameters for each cycle have to be treated separately. See details in supplemental information, Section S1.2.2.

(B) Partial ^{1}H NMR spectra (600 MHz, D_2O, pD = 13, 298 K) of the dynamic NMR experiments carried out on the first (left), second (middle), and third (right) operations on **DP** show that the characteristic resonances for the methine protons on **CB7**s/CB7s change with time. Signals of **CB7**s/CB7s in different chemical environments are differentiated by color: black (unbound), orange (CB7s encircling the deprotonated pumping cassette), green (CB7s residing on the collecting chain closest to a bound pumping cassette in the intermediate states **D[n]R-II**), cyan (CB7s residing on the collecting chain closest to an unbound pumping cassette), purple (CB7s residing on the collecting chain closest to a bound pumping cassette in the initial states **D[n]R-I**), and deep red (CB7s residing in the middle of the collecting chains). The first and second pumping cycles lead to complete loading of the CB7 rings onto the PEG collecting chains, while the third cycle results in an equilibrium state between **D[7]R-II** and **D[7]R**.

with four CB7 rings mechanically interlocked onto the PEG collecting chain as indicated by integrating the proton resonances (Figure S113) arising from the ring and dumbbell components. The activation barriers for the third and fourth rings passing over the TFP steric barriers increase very slightly as compared with the first cycle, which are found to be $\Delta G^{\ddagger}_3$ = 22.6 kcal mol^{-1} and $\Delta G^{\ddagger}_4$ = 22.8 kcal mol^{-1}, respectively, under pD = 13. HRMS offered further characterizations for both **D[3]R** and **D[5]R**, which formed clusters with multiple Na^+ ions in the gas phase. We attribute this observation to the presence of mobile CB7 rings threaded on the PEG chain, whose carbonyl portals serve as multidentate chelating sites for sodium cations. This interpretation was subsequently corroborated by molecular dynamics (MD) simulations (Figure S133).

After the third pumping cycle, however, the ^{1}H (and ^{19}F) NMR spectra (Figures 4B and S120–S122) reveal, by the presence of

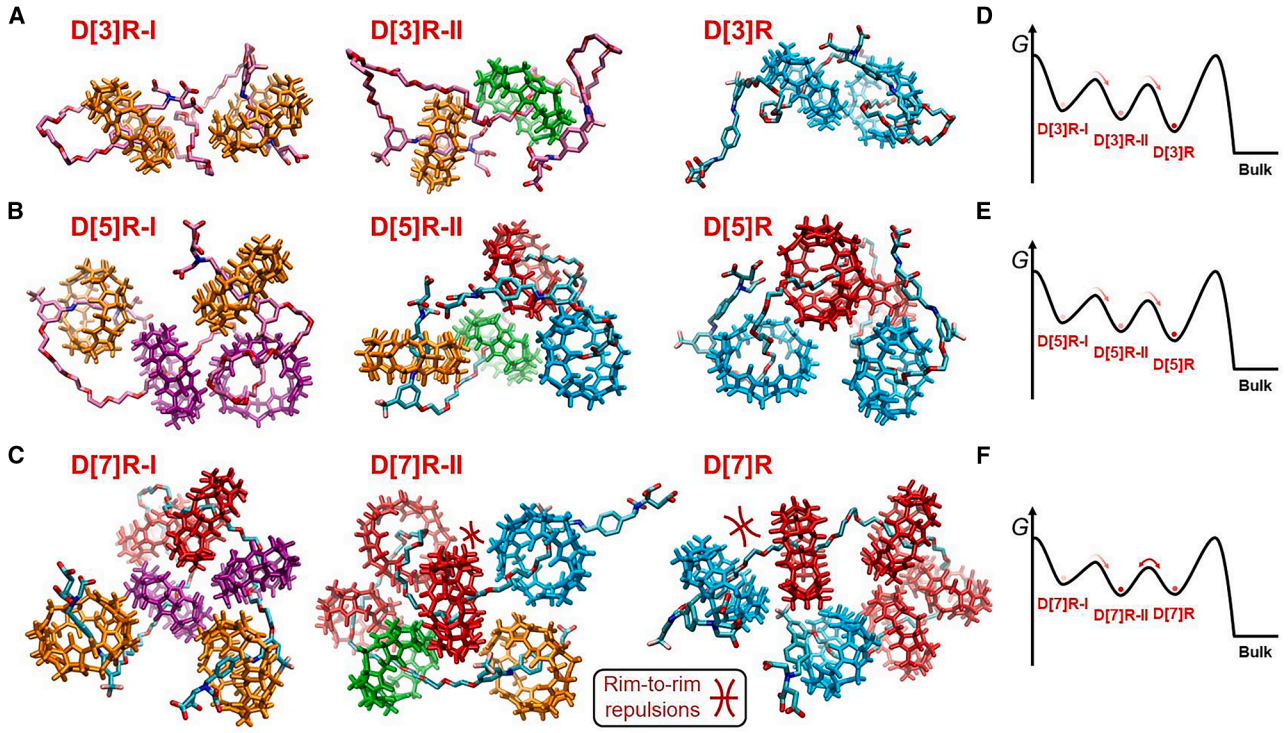

Figure 5. Equilibrated co-conformations at each stage over three pumping cycles on DP

(A–C) MD simulated structures for the equilibrated co-conformations of **D[3]R-I**, **D[3]R-II**, and **D[3]R** (from left to right and similarly hereinafter) for the first cycle (A); **D[5]R-I**, **D[5]R-II**, and **D[5]R** for the second cycle (B); and **D[7]R-I**, **D[7]R-II**, and **D[7]R** for the third cycle (C). The CB7 rings are labeled with different colors in accord with the colors of the stars used in Figure 4 to label the positions of the CB7 rings on the dumbbells. Hydrogen atoms on the dumbbells, counterions, and solvent molecules are omitted for the sake of clarity.

(D–F) Energy landscapes representing the relative free energies of each co-conformation for the first (D), second (E), and third (F) pumping cycles.

two sets of resonances, that there are two distinct species in equilibrium with one another after more than 24 h following the addition of base. The constant integrated area under the resonances of the methine protons from the CB7 rings trapped on the dumbbell during the whole process rules out the possibility that rings dethread over the pumping cassettes back into the bulk solution. Based on a 1:2 ratio between the integrated values for the bound and unbound pumping cassettes, we inferred that the two species existing after the third pumping cycle are **D[7]R-II** and **D[7]R**, with five and six CB7 rings positioned on the PEG collecting chain, respectively, in a 2:1 molar ratio. This observation implies that a PEG collecting chain consisting of 24 repeating units can accommodate a maximum of six CB7 rings under the condition of pumping studied. Nonetheless, the activation barrier for the fifth ring to pass over the steric barrier is only 23.0 kcal mol^{-1} under pD = 13, very similar to the value obtained for the fourth one. This observation infers that by increasing the length of the PEG collecting chain, it should be possible to synthesize polyrotaxanes with well-defined numbers of mechanically interlocked rings with even more than six rings using the well-established code of pumping.

MD simulations

Our chemical intuition regarding the mechanism by which pumping operates and our understanding of the interplay between kinetic and thermodynamic features were investigated using MD simulations of each co-conformation occurring during the three pumping cycles (see Videos S1, S2, and S3). Utilizing van der Waals and torsion parameters (see supplemental information, Section S8) optimized to align with quantum mechanics (QM) calculations, we were able to investigate the co-conformational changes (Figures 5A–5C) occurring during each cycle. These investigations reveal that co-conformational adjustments of the collecting chains enhance the interactions between the CB7 rings and the dumbbell. Specifically, before the first cycle, the collecting chain of **DP** forms a coiled conformation and stacks with the hydrophobic part of the pumping cassette, maximizing van der Waals interactions. This conformation is consistent with the relatively small average radius of gyration ($\langle R_g \rangle$) of 8.4 Å (Figure S131). Pumping of two CB7 rings onto the PEG collecting chain results in an extension of the dumbbell conformation such that $\langle R_g \rangle$ increases to 11.5 Å (**D[3]R**), providing room for the rings. The size of rotaxane continues to increase in a stepwise manner as more and more CB7 rings are loaded onto the collecting chain with an increase in $\langle R_g \rangle$ from 13.3 (**D[5]R**) to 14.0 Å (**D[7]R**). This tendency aligns with the results obtained from DOSY experiments. The average volume of 1.27×10^4 $Å^3$ for **D[7]R**, which is also obtained from the MD simulations, corresponds to a local concentration of 0.78 M for the six CB7 rings located on the dumbbell, *ca.* 350 times higher than the concentration (2.2 mM) of **CB7**

in the bulk solution. This concentration difference shows unambiguously the buildup of chemical potential of CB7 rings on the collecting chain relative to the **CB7** in the bulk solution.

Notably, the simulations reveal that even when the PEG collecting chain is saturated with six CB7 rings, the dumbbell never adopts a fully extended conformation during the pumping process. We hypothesize that this conformational preference results from the fact that CB7 rings tend to pack by nonspecific dipole-dipole and hydrophobic interactions. Given that the carbonyl portals and the equatorial methine groups of CB7 rings are electrostatically complementary, the spatially adjacent CB7 rings are apt to form an offset close contact. When more than five CB7 rings are trapped on the PEG collecting chain, however, a rim-to-rim alignment of neighboring rings becomes inevitable (Figure 5C) because of the limited space, which generates sizable electrostatic repulsion (Table S5) leading to the loss of stability of co-conformations. This progression, combined with the exothermic relocation of CB7 rings from the deprotonated pumping cassettes, explains why the third pumping cycle leads to an equilibrium between **D[7]R-II** and **D[7]R** (Figure 5F), where the former is favored over the latter (Table S4). The cycle-dependent evolution of these interactions underscores the intricate balance between the co-conformational adaptability and saturation of the pairwise interactions (Table S5) between the CB7 rings on the PEG collecting chain, enabling the molecular structures that confer the highest degree of stability under the conditions studied to be pinpointed.

Conclusions

We have demonstrated that in the course of harnessing chemical energy[77–79] provided by acid-base pulsing, rationally designed AMPs operating in water can drive the active transport of **CB7** rings—biocompatible macrocycles with potential pharmaceutical values[80]—onto polyethylene glycol chains, which have negligible affinity for the rings, with local concentrations up to 350 times higher than in the bulk. This highly efficient non-equilibrium assembling is achieved with perfect precision through simple pH modulation. Computational investigations have been conducted along with detailed kinetic studies to offer quantitative insights into the incorporated kinetic asymmetry and the resulting progressively endergonic pumping. This investigation provides a blueprint for the design of aqueous-based AMPs capable of installing precise numbers of rings on collecting chains to form non-equilibrium oligorotaxanes, contributing to the ongoing challenge of realizing life-mimicking endergonic synthesis[81] of polymeric materials in biologically relevant conditions.

METHODS

Further details regarding the methods can be found in the supplemental information.

RESOURCE AVAILABILITY

Lead contact

Further information and requests for resources and reagents should be directed to and will be fulfilled by the lead contact, Guangcheng Wu (gcwu2023@hku.hk).

Materials availability

All materials associated with the paper are either commercially available or can be prepared as indicated in the supplemental information, where full experimental details and characterization data are included.

Data and code availability

All data needed to support the conclusions of this manuscript are included in the main text or supplemental information. This paper does not report original code. Any additional information required to reanalyze the data reported in this paper is available from the lead contact upon request.

ACKNOWLEDGMENTS

We acknowledge the Integrated Molecular Structure Education and Research Center (IMSERC) at Northwestern University (NU) for providing access to equipment for relevant experiments. We are grateful for the access to the research facilities in the Chemistry Department of the University of Hong Kong (HKU). We thank NU and HKU for their continued support of this research. The usage of instruments in IMSERC receives support from the Soft and Hybrid Nanotechnology Experimental (SHyNE) Resource (NSF ECCS-2025633). G.W. acknowledges UGC funding administered by the University of Hong Kong for supporting the Electrospray Ionization Quadrupole Time-of-Flight Mass Spectrometry Facilities under the Support for Interdisciplinary Research in Chemical Science. W.A.G. and W.-G.L. thank NSF (CBET 2311117) and NIH (R01HL155532) for support. J.P., T.J., M.M.K., and H.K. acknowledge the National Research Foundation of Korea (NRF) grants funded by the Korean Government (MSIT) (no. RS-2024-00405261).

AUTHOR CONTRIBUTIONS

G.W., Y.J., and J.F.S. conceived the idea and designed the project; G.W. synthesized the compounds and performed the experiments with the help of Y.J., L.Z., B.S., and Q.L.; J.P., W.-G.L., T.J., M.M.K., H.K., and W.A.G. performed QM calculations and MD simulations. The manuscript was initially composed by G.W., J.P., R.D.A., W.A.G., and J.F.S., and all authors further contributed to the discussion of the experimental work and the final version of the manuscript.

DECLARATION OF INTERESTS

The authors declare no competing interests.

SUPPLEMENTAL INFORMATION

Supplemental information can be found online at https://doi.org/10.1016/j.chempr.2025.102878.

Received: July 14, 2025
Revised: October 1, 2025
Accepted: November 24, 2025

REFERENCES

1. Schrödinger, E. (1944). What Is Life? The Physical Aspect of the Living Cell (Cambridge University Press).
2. Fletcher, S.P., Dumur, F., Pollard, M.M., and Feringa, B.L. (2005). A reversible, unidirectional molecular rotary motor driven by chemical energy. Science *310*, 80–82. https://doi.org/10.1126/science.1117090.
3. Serreli, V., Lee, C.F., Kay, E.R., and Leigh, D.A. (2007). A molecular information ratchet. Nature *445*, 523–527. https://doi.org/10.1038/nature05452.
4. Li, H., Cheng, C., McGonigal, P.R., Fahrenbach, A.C., Frasconi, M., Liu, W.G., Zhu, Z., Zhao, Y., Ke, C., Lei, J., et al. (2013). Relative unidirectional translation in an artificial molecular assembly fueled by light. J. Am. Chem. Soc. *135*, 18609–18620. https://doi.org/10.1021/ja4094204.

5. Erbas-Cakmak, S., Fielden, S.D.P., Karaca, U., Leigh, D.A., McTernan, C.T., Tetlow, D.J., and Wilson, M.R. (2017). Rotary and linear molecular motors driven by pulses of a chemical fuel. Science *358*, 340–343. https://doi.org/10.1126/science.aao1377.

6. Borsley, S., Kreidt, E., Leigh, D.A., and Roberts, B.M.W. (2022). Autonomous fuelled directional rotation about a covalent single bond. Nature *604*, 80–85. https://doi.org/10.1038/s41586-022-04450-5.

7. Zhang, L., Qiu, Y., Liu, W.G., Chen, H., Shen, D., Song, B., Cai, K., Wu, H., Jiao, Y., Feng, Y., et al. (2023). An electric molecular motor. Nature *613*, 280–286. https://doi.org/10.1038/s41586-022-05421-6.

8. Liu, E., Cherraben, S., Boulo, L., Troufflard, C., Hasenknopf, B., Vives, G., and Sollogoub, M. (2023). A molecular information ratchet using a cone-shaped macrocycle. Chem *9*, 1147–1163. https://doi.org/10.1016/j.chempr.2022.12.017.

9. Zwick, P., Troncossi, A., Borsley, S., Vitorica-Yrezabal, I.J., and Leigh, D.A. (2024). Stepwise operation of a molecular rotary motor driven by an appel reaction. J. Am. Chem. Soc. *146*, 4467–4472. https://doi.org/10.1021/jacs.3c10266.

10. Liu, E., Daou, D., Hasenknopf, B., Vives, G., and Sollogoub, M. (2025). Not going back: Unidirectional movement by intramolecular one-way ratcheting of functionalized cyclodextrin. Chem *11*, 102623. https://doi.org/10.1016/j.chempr.2025.102623.

11. Koumura, N., Zijlstra, R.W.J., van Delden, R.A., Harada, N., and Feringa, B.L. (1999). Light-driven monodirectional molecular rotor. Nature *401*, 152–155. https://doi.org/10.1038/43646.

12. Koumura, N., Geertsema, E.M., van Gelder, M.B., Meetsma, A., and Feringa, B.L. (2002). Second generation light-driven molecular motors. Unidirectional rotation controlled by a single stereogenic center with near-perfect photoequilibria and acceleration of the speed of rotation by structural modification. J. Am. Chem. Soc. *124*, 5037–5051. https://doi.org/10.1021/ja012499i.

13. Baroncini, M., Silvi, S., Venturi, M., and Credi, A. (2012). Photoactivated directionally controlled transit of a non-symmetric molecular axle through a macrocycle. Angew. Chem. Int. Ed. Engl. *51*, 4223–4226. https://doi.org/10.1002/anie.201200555.

14. Greb, L., and Lehn, J.-M. (2014). Light-driven molecular motors: Imines as four-step or two-step unidirectional rotors. J. Am. Chem. Soc. *136*, 13114–13117. https://doi.org/10.1021/ja506034n.

15. Kistemaker, J.C.M., Štacko, P., Visser, J., and Feringa, B.L. (2015). Unidirectional rotary motion in achiral molecular motors. Nat. Chem. *7*, 890–896. https://doi.org/10.1038/nchem.2362.

16. Ragazzon, G., Baroncini, M., Silvi, S., Venturi, M., and Credi, A. (2015). Light-powered autonomous and directional molecular motion of a dissipative self-assembling system. Nat. Nanotechnol. *10*, 70–75. https://doi.org/10.1038/nnano.2014.260.

17. Kassem, S., van Leeuwen, T., Lubbe, A.S., Wilson, M.R., Feringa, B.L., and Leigh, D.A. (2017). Artificial molecular motors. Chem. Soc. Rev. *46*, 2592–2621. https://doi.org/10.1039/c7cs00245a.

18. Baroncini, M., Silvi, S., and Credi, A. (2020). Photo- and redox-driven artificial molecular motors. Chem. Rev. *120*, 200–268. https://doi.org/10.1021/acs.chemrev.9b00291.

19. Cheng, C., McGonigal, P.R., Schneebeli, S.T., Li, H., Vermeulen, N.A., Ke, C., and Stoddart, J.F. (2015). An artificial molecular pump. Nat. Nanotechnol. *10*, 547–553. https://doi.org/10.1038/nnano.2015.96.

20. Qiu, Y., Song, B., Pezzato, C., Shen, D., Liu, W., Zhang, L., Feng, Y., Guo, Q.-H., Cai, K., Li, W., et al. (2020). A precise polyrotaxane synthesizer. Science *368*, 1247–1253. https://doi.org/10.1126/science.abb3962.

21. Amano, S., Fielden, S.D.P., and Leigh, D.A. (2021). A catalysis-driven artificial molecular pump. Nature *594*, 529–534. https://doi.org/10.1038/s41586-021-03575-3.

22. Binks, L., Tian, C., Fielden, S.D.P., Vitorica-Yrezabal, I.J., and Leigh, D.A. (2022). Transamidation-driven molecular pumps. J. Am. Chem. Soc. *144*, 15838–15844. https://doi.org/10.1021/jacs.2c06807.

23. Li, A., Tan, Z., Hu, Y., Lu, Z., Yuan, J., Li, X., Xie, J., Zhang, J., and Zhu, K. (2022). Precise control of radial catenane synthesis via clipping and pumping. J. Am. Chem. Soc. *144*, 2085–2089. https://doi.org/10.1021/jacs.1c12303.

24. Qiu, Y., Feng, Y., Guo, Q.-H., Astumian, R.D., and Stoddart, J.F. (2020). Pumps through the ages. Chem *6*, 1952–1977. https://doi.org/10.1016/j.chempr.2020.07.009.

25. Zhang, L., Wu, H., Li, X., Chen, H., Astumian, R.D., and Stoddart, J.F. (2024). Artificial molecular pumps. Nat. Rev. Methods Primers *4*, 1–21. https://doi.org/10.1038/s43586-024-00291-w.

26. Szent-Györgyi, A. (1971). Biology and pathology of water. Perspect. Biol. Med. *14*, 239–249. https://doi.org/10.1353/pbm.1971.0014.

27. Franks, F. (2000). Water: A Matrix of Life (Royal Society of Chemistry).

28. Steinberg-Yfrach, G., Liddell, P.A., Hung, S.-C., Moore, A.L., Gust, D., and Moore, T.A. (1997). Conversion of light energy to proton potential in liposomes by artificial photosynthetic reaction centres. Nature *385*, 239–241. https://doi.org/10.1038/385239a0.

29. Steinberg-Yfrach, G., Rigaud, J.L., Durantini, E.N., Moore, A.L., Gust, D., and Moore, T.A. (1998). Light-driven production of ATP catalysed by F0F1-ATP synthase in an artificial photosynthetic membrane. Nature *392*, 479–482. https://doi.org/10.1038/33116.

30. Bennett, I.M., Farfano, H.M.V., Bogani, F., Primak, A., Liddell, P.A., Otero, L., Sereno, L., Silber, J.J., Moore, A.L., Moore, T.A., et al. (2002). Active transport of Ca2+ by an artificial photosynthetic membrane. Nature *420*, 398–401. https://doi.org/10.1038/nature01209.

31. Xie, X., Crespo, G.A., Mistlberger, G., and Bakker, E. (2014). Photocurrent generation based on a light-driven proton pump in an artificial liquid membrane. Nat. Chem. *6*, 202–207. https://doi.org/10.1038/nchem.1858.

32. Howe, E.N.W., and Gale, P.A. (2019). Fatty acid fueled transmembrane chloride transport. J. Am. Chem. Soc. *141*, 10654–10660. https://doi.org/10.1021/jacs.9b02116.

33. Pruchyathamkorn, J., Nguyen, B.T., Grommet, A.B., Novoveska, M., Ronson, T.K., Thoburn, J.D., and Nitschke, J.R. (2024). Harnessing Maxwell's demon to establish a macroscale concentration gradient. Nat. Chem. *16*, 1558–1564. https://doi.org/10.1038/s41557-024-01549-2.

34. Shao, B., Fu, H., and Aprahamian, I. (2024). A molecular anion pump. Science *385*, 544–549. https://doi.org/10.1126/science.adp3506.

35. Kriebisch, C.M.E., Kriebisch, B.A.K., Häfner, G., Soria-Carrera, H., Fei, Y., Müller, M., and Boekhoven, J. (2025). Chemically Fueled Active Transport. Angew. Chem. Int. Ed. Engl. *64*, e202500243. https://doi.org/10.1002/anie.202500243.

36. Liang, K., Nicoli, F., Shehimy, S.A., Penocchio, E., Di Noja, S., Li, Y., Bonfio, C., Borsley, S., and Ragazzon, G. (2025). Catalysis-driven active transport across a liquid membrane. Angew. Chem. Int. Ed. Engl. *64*, e202421234. https://doi.org/10.1002/anie.202421234.

37. Borsley, S., Leigh, D.A., and Roberts, B.M.W. (2021). A Doubly Kinetically-Gated Information Ratchet Autonomously Driven by Carbodiimide Hydration. J. Am. Chem. Soc. *143*, 4414–4420. https://doi.org/10.1021/jacs.1c01172.

38. Borsley, S., Leigh, D.A., Roberts, B.M.W., and Vitorica-Yrezabal, I.J. (2022). Tuning the force, speed, and efficiency of an autonomous chemically fueled information ratchet. J. Am. Chem. Soc. *144*, 17241–17248. https://doi.org/10.1021/jacs.2c07633.

39. Binks, L., Borsley, S., Gingrich, T.R., Leigh, D.A., Penocchio, E., and Roberts, B.M.W. (2023). The role of kinetic asymmetry and power strokes in an information ratchet. Chem *9*, 2902–2917. https://doi.org/10.1016/j.chempr.2023.05.035.

40. Gallagher, J.M., Roberts, B.M.W., Borsley, S., and Leigh, D.A. (2024). Conformational selection accelerates catalysis by an organocatalytic molecular motor. Chem *10*, 855–866. https://doi.org/10.1016/j.chempr.2023.10.019.

41. Liu, H.K., Mrad, T.W., Troncossi, A., Borsley, S., Roberts, B.M.W., Betts, A., and Leigh, D.A. (2025). Structural influence of the chemical fueling system on a catalysis-driven rotary molecular motor. J. Am. Chem. Soc. *147*, 8785–8795. https://doi.org/10.1021/jacs.5c00028.

42. Berreur, J., Watts, O.F.B., Bulless, T.H.N., O'Donoghue, N.T., Del Olmo, M., Winter, A.J., Clayden, J., and Collins, B.S.L. (2025). Redox-powered autonomous directional C-C bond rotation under enzyme control. Nature *644*, 96–101. https://doi.org/10.1038/s41586-025-09291-6.

43. Liu, K., Blokhuis, A.W.P., Dijt, S.J., Wu, J., Hamed, S., Kiani, A., Matysiak, B.M., and Otto, S. (2025). Molecular-scale dissipative chemistry drives the formation of nanoscale assemblies and their macroscale transport. Nat. Chem. *17*, 124–131. https://doi.org/10.1038/s41557-024-01665-z.

44. Wang, P.L., Borsley, S., Power, M.J., Cavasso, A., Giuseppone, N., and Leigh, D.A. (2025). Transducing chemical energy through catalysis by an artificial molecular motor. Nature *637*, 594–600. https://doi.org/10.1038/s41586-024-08288-x.

45. van Dijken, D.J., Chen, J., Stuart, M.C.A., Hou, L., and Feringa, B.L. (2016). Amphiphilic molecular motors for responsive aggregation in water. J. Am. Chem. Soc. *138*, 660–669. https://doi.org/10.1021/jacs.5b11318.

46. Lubbe, A.S., Böhmer, C., Tosi, F., Szymanski, W., and Feringa, B.L. (2018). Molecular motors in aqueous environment. J. Org. Chem. *83*, 11008–11018. https://doi.org/10.1021/acs.joc.8b01627.

47. Xu, F., Crespi, S., Pacella, G., Fu, Y., Stuart, M.C.A., Zhang, Q., Portale, G., and Feringa, B.L. (2022). Dynamic control of a multistate chiral supramolecular polymer in water. J. Am. Chem. Soc. *144*, 6019–6027. https://doi.org/10.1021/jacs.2c01063.

48. Carter, N.J., and Cross, R.A. (2005). Mechanics of the kinesin step. Nature *435*, 308–312. https://doi.org/10.1038/nature03528.

49. Rodnina, M.V. (2023). Decoding and recoding of mRNA sequences by the ribosome. Annu. Rev. Biophys. *52*, 161–182. https://doi.org/10.1146/annurev-biophys-101922-072452.

50. Luo, J., Huang, C., Liao, Z., Ma, X., Si, T., Chen, H., Li, Z., and Fan, J. (2025). Unidirectional drug delivery and responsive release guided by nanofunnel-shaped heterojunction. Nano Lett. *25*, 7853–7859. https://doi.org/10.1021/acs.nanolett.5c00617.

51. Herges, R. (2020). Molecular assemblers: Molecular machines performing chemical synthesis. Chem. Sci. *11*, 9048–9055. https://doi.org/10.1039/d0sc03094e.

52. Reimann, P. (2002). Brownian motors: Noisy transport far from equilibrium. Phys. Rep. *361*, 57–265. https://doi.org/10.1016/S0370-1573(01)00081-3.

53. Astumian, R.D. (2007). Design principles for Brownian molecular machines: How to swim in molasses and walk in a hurricane. Phys. Chem. Chem. Phys. *9*, 5067–5083. https://doi.org/10.1039/b708995c.

54. Parrondo, J.M.R., and de Cisneros, B.J. (2014). Energetics of Brownian motors: A review. Appl. Phys., A *75*, 179–191. https://doi.org/10.1007/s003390201332.

55. Astumian, R.D. (2024). Kinetic asymmetry and directionality of nonequilibrium molecular systems. Angew. Chem. Int. Ed. Engl. *63*, e202306569. https://doi.org/10.1002/anie.202306569.

56. Lee, C.K., Feng, Y., Enciso, A.E., Violi, J.P., Donald, W.A., Stoddart, J.F., and Kim, D.J. (2025). An aqueous artificial molecular pump. Chem *12*, 102693. https://doi.org/10.1016/j.chempr.2025.102693.

57. Pezzato, C., Nguyen, M.T., Cheng, C., Kim, D.J., Otley, M.T., and Stoddart, J.F. (2017). An efficient artificial molecular pump. Tetrahedron *73*, 4849–4857. https://doi.org/10.1016/j.tet.2017.05.087.

58. Astumian, R.D., and Derényi, I. (1998). Fluctuation driven transport and models of molecular motors and pumps. Eur. Biophys. J. *27*, 474–489. https://doi.org/10.1007/s002490050158.

59. Borsley, S., Leigh, D.A., and Roberts, B.M.W. (2024). Molecular ratchets and kinetic asymmetry: Giving chemistry direction. Angew. Chem. Int. Ed. Engl. *63*, e202400495. https://doi.org/10.1002/anie.202400495.

60. Kim, J., Jung, I.-S., Kim, S.-Y., Lee, E., Kang, J.-K., Sakamoto, S., Yamaguchi, K., and Kim, K. (2000). New cucurbituril homologues: Syntheses, isolation, characterization, and X-ray crystal structures of cucurbit[n]uril (n = 5, 7, and 8). J. Am. Chem. Soc. *122*, 540–541. https://doi.org/10.1021/ja993376p.

61. Lee, J.W., Samal, S., Selvapalam, N., Kim, H.-J., and Kim, K. (2003). Cucurbituril homologues and derivatives: New opportunities in supramolecular chemistry. Acc. Chem. Res. *36*, 621–630. https://doi.org/10.1021/ar020254k.

62. Lagona, J., Mukhopadhyay, P., Chakrabarti, S., and Isaacs, L. (2005). The cucurbit[n]uril family. Angew. Chem. Int. Ed. Engl. *44*, 4844–4870. https://doi.org/10.1002/anie.200460675.

63. Assaf, K.I., and Nau, W.M. (2015). Cucurbiturils: From synthesis to high-affinity binding and catalysis. Chem. Soc. Rev. *44*, 394–418. https://doi.org/10.1039/c4cs00273c.

64. Barrow, S.J., Kasera, S., Rowland, M.J., del Barrio, J., and Scherman, O.A. (2015). Cucurbituril-based molecular recognition. Chem. Rev. *115*, 12320–12406. https://doi.org/10.1021/acs.chemrev.5b00341.

65. Freeman, W.A., Mock, W.L., and Shih, N.Y. (1981). Cucurbituril. J. Am. Chem. Soc. *103*, 7367–7368. https://doi.org/10.1021/ja00414a070.

66. Rekharsky, M.V., Mori, T., Yang, C., Ko, Y.H., Selvapalam, N., Kim, H., Sobransingh, D., Kaifer, A.E., Liu, S., Isaacs, L., et al. (2007). A synthetic host-guest system achieves avidin-biotin affinity by overcoming enthalpy–entropy compensation. Proc. Natl. Acad. Sci. USA *104*, 20737–20742. https://doi.org/10.1073/pnas.0706407105.

67. Sobransingh, D., and Kaifer, A.E. (2005). Binding interactions between the host cucurbit[7]uril and dendrimer guests containing a single ferrocenyl residue. Chem. Commun., 5071–5073. https://doi.org/10.1039/b510780f.

68. Kaifer, A.E., Li, W., Silvi, S., and Sindelar, V. (2012). Pronounced pH effects on the kinetics of cucurbit[7]uril-based pseudorotaxane formation and dissociation. Chem. Commun. *48*, 6693–6695. https://doi.org/10.1039/c2cc32871b.

69. Neira, I., García, M.D., Peinador, C., and Kaifer, A.E. (2019). Terminal carboxylate effects on the thermodynamics and kinetics of cucurbit[7]uril binding to guests containing a central bis(pyridinium)-xylylene site. J. Org. Chem. *84*, 2325–2329. https://doi.org/10.1021/acs.joc.8b02993.

70. Zheng, Y., and Kaifer, A.E. (2020). Kinetics and thermodynamics of binding between zwitterionic viologen guests and the cucurbit[7]uril host. J. Org. Chem. *85*, 10240–10244. https://doi.org/10.1021/acs.joc.0c01201.

71. Yang, X., Cheng, Q., Monnier, V., Charles, L., Karoui, H., Ouari, O., Gigmes, D., Wang, R., Kermagoret, A., and Bardelang, D. (2021). Guest exchange by a partial energy ratchet in water. Angew. Chem. Int. Ed. Engl. *60*, 6617–6623. https://doi.org/10.1002/anie.202014399.

72. Wang, Z., Sun, C., Yang, K., Chen, X., and Wang, R. (2022). Cucurbituril-based supramolecular polymers for biomedical applications. Angew. Chem. Int. Ed. Engl. *61*, e202206763. https://doi.org/10.1002/anie.202206763.

73. Kim, K., Selvapalam, N., Ko, Y.H., Park, K.M., Kim, D., and Kim, J. (2007). Functionalized cucurbiturils and their applications. Chem. Soc. Rev. *36*, 267–279. https://doi.org/10.1039/b603088m.

74. Yin, H., Cheng, Q., Bardelang, D., and Wang, R. (2023). Challenges and opportunities of functionalized cucurbiturils for biomedical applications. JACS Au *3*, 2356–2377. https://doi.org/10.1021/jacsau.3c00273.

75. Wang, W., Wang, X., Cao, J., Liu, J., Qi, B., Zhou, X., Zhang, S., Gabel, D., Nau, W.M., Assaf, K.I., et al. (2018). The chaotropic effect as an orthogonal assembly motif for multi-responsive dodecaborate-cucurbituril supramolecular networks. Chem. Commun. *54*, 2098–2101. https://doi.org/10.1039/c7cc08078f.

76. Astumian, R.D., and Robertson, B. (1993). Imposed oscillations of kinetic barriers can cause an enzyme to drive a chemical reaction away from equilibrium. J. Am. Chem. Soc. *115*, 11063–11068. https://doi.org/10.1021/ja00077a001.

77. Ragazzon, G., and Prins, L.J. (2018). Energy consumption in chemical fuel-driven self-assembly. Nat. Nanotechnol. *13*, 882–889. https://doi.org/10.1038/s41565-018-0250-8.

78. Weißenfels, M., Gemen, J., and Klajn, R. (2021). Dissipative self-assembly: Fueling with chemicals versus light. Chem *7*, 23–37. https://doi.org/10.1016/j.chempr.2020.11.025.

79. Borsley, S., Leigh, D.A., and Roberts, B.M.W. (2022). Chemical fuels for molecular machinery. Nat. Chem. *14*, 728–738. https://doi.org/10.1038/s41557-022-00970-9.

80. Jones, L.M., Super, E.H., Batt, L.J., Gasbarri, M., Coppola, F., Bhebhe, L.M., Cheesman, B.T., Howe, A.M., Král, P., Coulston, R., et al. (2022). Broad-spectrum extracellular antiviral properties of cucurbit[n]urils. ACS Infect. Dis. *8*, 2084–2095. https://doi.org/10.1021/acsinfecdis.2c00186.

81. Olivieri, E., Gallagher, J.M., Betts, A., Mrad, T.W., and Leigh, D.A. (2024). Endergonic synthesis driven by chemical fuelling. Nat. Synth. *3*, 707–714. https://doi.org/10.1038/s44160-024-00493-w.

Chem

Article

Precise synthesis of non-equilibrium rotaxanes via pumping in water

Graphical abstract

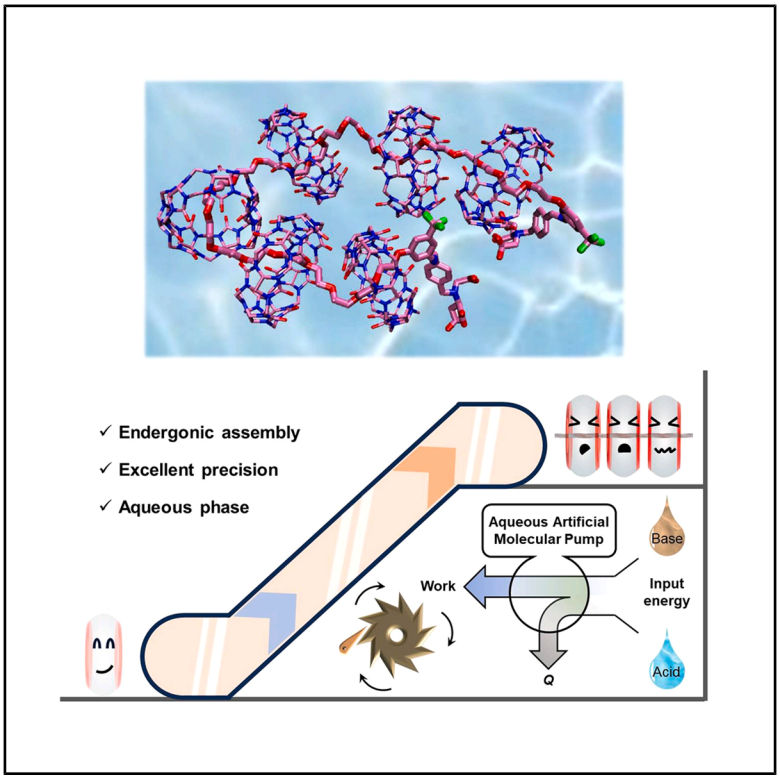

Highlights

- An artificial molecular pump has been designed to operate efficiently in pure water
- Neutralization energy is harnessed to precisely install rings onto a polymer chain
- Non-equilibrium mechanically interlocked polymers are facilely synthesized
- Co-conformation is governed by intercomponent interactions within the rotaxane

Authors

Guangcheng Wu, Jihye Park, Wei-Guang Liu, ..., R. Dean Astumian, William A. Goddard III, J. Fraser Stoddart

Correspondence

gcwu2023@hku.hk (G.W.), astumian@maine.edu (R.D.A.), wag@caltech.edu (W.A.G.), stoddart@hku.hk (J.F.S.)

In brief

The realization of artificial molecular pumps (AMPs) that function in water remains challenging. The authors report a rationally designed aqueous AMP with brand-new ratchet components. Powered by acid-base pulses, it drives the non-equilibrium synthesis of well-defined interlocked polymers, achieving a local cucurbit[7]uril concentration 350 times higher than in bulk solution.

Wu et al., 2026, Chem *12*, 102878
April 9, 2026
https://doi.org/10.1016/j.chempr.2025.102878

CellPress